Title: From flowering to foliage: Accelerometers track tree sway to provide high-resolution insights into tree phenology

Authors: Jaeger, D.M.[a,b*], Looze, A.C.M.[a], Raleigh, M.S.[c], Miller, B.W.[d], Friedman, J.M.[e], Wessman, C.A.[a,b]

*corresponding author: deidre.jaeger@colorado.edu

Affiliations: [a]Department of Ecology and Evolutionary Biology, University of Colorado, Boulder, CO 80309, [b]Cooperative Institute for Research in Environmental Sciences, University of Colorado, Boulder CO 80309, [c]College of Earth, Ocean, and Atmospheric Sciences, Oregon State University, Corvallis, OR, 97331, [d]U.S. Geological Survey, North Central Climate Adaptation Science Center, Fort Collins, CO, 80526, [e]Fort Collins Science Center, US Geological Survey, Ft. Collins, CO 80526

Abstract: Trees are bioindicators of global climate change and regional urbanization, but available monitoring tools are ineffective for fine-scale observation of many species. Using six accelerometers mounted on two urban ash trees (*Fraxinus americana*), we looked at high-frequency tree vibrations, or change in periodicity of tree sway as a proxy for mass changes, to infer seasonal patterns of flowering and foliage (phenophases). We compared accelerometer-estimated phenophases to those derived from digital repeat photography using Green Chromatic Coordinates (GCC) and visual observation of phenophases defined by the USA National Phenology Network (NPN). We also drew comparisons between two commercial accelerometers and assessed how placement height influenced the ability to extract seasonal transition dates. Most notably, tree sway data showed a greenness signal in an urban environment and produced a clear flowering time-series and peak flowering signal (PF), marking the first observations of a flower phenophase using accelerometer data. Estimated start of

spring (SOS) from accelerometers and time-lapse GCC were more similar than start of autumn (SOA); accelerometers lagged behind the time-lapse camera dates by three and four days for SOS and 13 and 14 days for SOA for each tree. Estimates for SOS and SOA from accelerometers and time-lapse cameras aligned closely with different NPN phenophases. The two commercial accelerometers produced similar season onset: a difference of 2.4 to 3.8 days for SOS, 2.1 days for SOA, and 0.5 to 2.0 days for PF. Accelerometers placed at the main crown branch point versus higher in the canopy showed a difference of 0.2 to 4.9 days for SOS and -1.5 to 1.7 days for PF. Our results suggest accelerometers present a novel opportunity to objectively monitor reproductive tree biology and fill gaps in phenology observations. Furthermore, widely available accelerometers show promise for scaling up from individual trees to the landscape level to aid forest management and assessing climate change impacts to tree phenology.

Keywords:

plant phenology, accelerometers, digital repeat photography, *Fraxinus americana*, tree sway, urban forests

1. Introduction

Changes in seasonal growth cycles of trees, or tree phenology, have consequences across a broad range of sectors, from wildlife to hydrology to human health and well-being. For wildlife, shifting tree phenology has strong links with herbivory (Korösi et al. 2018), habitat provisioning (Evans et al. 2016), migratory patterns (Tryjnowski et al. 2013), and community level interactions (Primack et al. 2009; Walther et al. 2002). For humans, altered tree phenology influences water movement and infiltration (Xiao and McPherson 2002), cooling capacity

(Stanley et al. 2019) and other ecosystem services (Tzoulas et al. 2007). In particular, the timing of flowering is important for numerous ecological and socio-economic reasons. For example, floral timing influences activity of nectar-gathering insects (Gérard et al. 2020) and influences vulnerability to damaging weather events (Hufkens et al. 2012). Flowering also impacts allergen prevalence (Jochner et al. 2013;Traidl-Hoffmann et al. 2003), human psycho-emotional well-being (Cameron et al. 2012; Burroughs 2002), tourism (Wang et al. 2017), aesthetics (Kareiva et al. 2007), and agriculture (Duraiappah et al. 2005; Menzel 2002). Given that climate change and densification of cities is likely to continue to impact the drivers of tree phenology such as air temperatures, it is vital to have tree monitoring tools to understand the trends and intensity of both foliar and floral shifts in trees.

While the scientific community has made great strides in studying the relationships between climate and tree phenology through remote-sensing methods (Li et al. 2017; Klosterman et al. 2014; Cleland et al. 2007) and in making connections across observation platforms (Richardson et al. 2017; Schwartz and Hanes 2010; Fisher et al. 2005; Morisette et al. 2021), challenges remain (Park et al. 2021; Morisette et al. 2009). In some environments (e.g., urban forests), observation tools that may be suitable for continuous forest are not effective given the diversity of tree species and the matrix of trees, other vegetation, and the built environment that may be found within a single satellite pixel. For example, imagery is available through no-cost government-operated data portals with temporal resolution on the order of days (e.g., MODIS), but the spatial resolution of these sources may not be sufficient for some settings and applications. Sensors on privately-managed satellites have the ability to capture high spatial resolution, on the order of 30 cm (Fang et al. 2020), with customized temporal coverage (DigitalGlobe Inc, 2016). However, there are significant cost barriers associated with purchasing imagery to observe multiple phenological events. Drone-based sensors also offer high spatial resolution phenological data (Klosterman et al. 2018), but obtaining permissions to fly above populated areas poses a hurdle to high-resolution temporal monitoring.

Given that species-level studies of tree phenology are constrained by the need for high spatial and temporal coverage (Yang et al. 2020; Badeck et al. 2004), species-specific phenological studies typically still rely on traditional labor-intensive visual observations in the field (Gray and Ewers 2021; Elmendorf et al. 2016; Wohlfahrt et al. 2019; Iler et al. 2013; Inouye 2008) or historical diaries (Fitchett and Raik 2021; Zheng et al. 2013). Visual observations are critical for gathering information about flowering phenophases as exemplified in the national launch of plant monitoring at National Ecological Observation Network sites (Elmendorf et al. 2016). When a single species dominates an area, a combination of remote- and ground-observation methods has been successful to understand tree phenology at the landscape level (Elmore et al. 2016); however, pixels with mixed-land use were not successful (Elmore et al. 2016) and in some cases comparison of these observation methods have shown opposite trends (Fu et al. 2014).

Digital repeat photography, also called time-lapse camera imagery, that estimates greenness (Klosterman et al. 2014) can be an effective tool for studying multiple tree species (Sonnentag et al. 2012), linking to satellite data (Yingying et al. 2018), and reducing human-based errors (Seyednasrollah et al. 2019). However, extending the geographic coverage of these phenology cameras can be expensive (in terms of camera-associated equipment) and logistically challenging. For example, ideal camera positioning is above the canopy pointing northward to avoid shadows in the field of view (Sunoj et al. 2016). Erecting towers is often not practical in the urban environment and repeat-photography in such settings raises privacy concerns. There may be opportunities to leverage existing imagery platforms such as camera infrastructure in cities (i.e., traffic monitoring cameras) or public posts on social media platforms to extract vegetation indices, though significant spatial and temporal resolution obstacles remain (Vaz et al. 2019; Morris et al. 2013). Despite the advances, sensor-based phenological studies (whether using near-surface or remotely-sensed data) are limited in their ability to capture some phenophases, such as the start and progression of flowering (Sunoj et al. 2016).

Scalable, non-invasive, inexpensive methods are needed for long-term vegetation monitoring, particularly in an urban environment. Novel methodology has emerged to infer seasonal tree patterns derived from accelerometer sensors. Accelerometers can detect patterns of vibrations of an object after a force sets the object in motion. A multi-axis accelerometer mounted to the surface of a tree trunk can detect the pattern of natural vibrations that the tree experiences due to wind or other forces (Jackson et al. 2021; Selker et al. 2011). The frequency of vibrations, or number of sway cycles per second, is inversely related to the tree's mass (van Emmerick et al. 2017; Moore and Maguire 2004; Baker 1997). Phenological changes in a tree may change its mass distribution or stiffness, altering the cycle period (and inversely, the frequency) (Bunce et al. 2019; Gougherty et al. 2018). Accelerometer data can be analyzed to extract the period length over time. The periods with the largest amplitude, called the dominant periods, can be assembled into a time-series and modeled to extract the onset of seasonal transitions (Gougherty et al. 2018).

Accelerometers show the potential to fill a niche in sensor-based approaches to monitoring tree phenology. Mass changes in plants have been used to answer questions of plant biomechanics by applying theory and tools on vibrations from the engineering field (de Langre 2019). Accelerometer-derived mass changes have been used to estimate tree properties such as drought stress (Ciruzzi and Loheide 2019; Sano et al. 2015), wind stress (Lohou et al. 2003), rain interception (van Emmerick et al. 2017; Selker et al. 2011), snow loading (Raleigh et al., 2021), buckling of branches (Timishenko and Gere, 2009), fruit ripening (Hou et al. 2018), and changes in foliage (Gougherty et al. 2018).

Many questions remain regarding which tree growth events can be tracked with accelerometers and which environments are conducive to detecting tree sway signals. For example, mass changes associated with tree flower emergence have not been studied with accelerometers. Additionally, studies looking at tree sway have targeted trees within continuous forests (Gougherty et al. 2018; van Emmerick et al. 2017). Despite indications that trees at the

130 forest edge or in the open can be successfully monitored with accelerometers (Gougherty et al.
131 2018), it is unknown whether there is sufficient wind forcing to study trees in an urban landscape
132 that has large structures that can shelter trees from wind. Given that canopy architecture varies
133 among deciduous tree species, phenology signals and placement height may be species-
134 specific. While wind more readily generates motion on secondary branches of the upper
135 canopy, sway signal has been detected from sensor placements as low as 1 meter from the
136 ground on the main trunk of some deciduous trees (Gougherty et al. 2018).
137 The purpose of this study was to test the ability to derive vegetation indices such as
138 foliage and flowering from accelerometers on trees in an urban setting. Our primary objective
139 was to build a growth curve from urban trees lining an urban sidewalk and address how
140 flowering and foliage dates derived from accelerometers compare to digital repeat photographs
141 and visual observations. Because connections between digital camera imagery and field
142 observations have been established and past studies have linked field observations to
143 accelerometer-derived vegetation indices, we hypothesized that both imagery and visual
144 observations would be comparable to the accelerometer estimates. On the other hand, because
145 accelerometers log variation in tree motion related to changing biomass while digital cameras
146 and humans collect visual data at intervals, accelerometers may provide complementary
147 information about tree activity by detecting different phenological stages or providing information
148 that is temporally offset from imagery or field observations.
149 Our secondary objective was to evaluate two practical aspects of accelerometer use. We
150 investigated how unit type and placement height influenced the ability to extract dates of
151 seasonal transitions in trees. To date, only one study has used accelerometers for estimating
152 tree phenology using custom-made devices for use on trees (Gougherty et al. 2018). We build
153 on their work and compare the custom sensor with an inexpensive and widely available
154 accelerometer marketed for a variety of motion detection applications. Given that
155 accelerometers should have similar functionality, we expected that different types of

accelerometers should detect a similar phenological growing season signal. For the question of height, we expected that placement on the main trunk at the tree crown should be sufficiently high for wind to induce a detectable signal. The purpose of these unit and height comparisons was to provide guidance on how to scale up the use of accelerometer monitoring in a feasible and cost-effective manner. To test this, we placed accelerometers at two different heights on two trees in an urban setting.

2. Material and Methods

2.1. Study species and location

We used two 30-year-old pollen-bearing white ash (*Fraxinus americana*) trees in Boulder, Colorado to study tree sway and phenology. White ash are wind-pollinated, dioecious (separate trees are pollen or fruit bearing), deciduous broadleaf trees with a natural range extending from the eastern United States forests to the Midwest plains. White ash trees provide significant shade (Poland and Mccullough 2006) and are planted in Colorado and other states by the thousands to millions along streets and in greenspace (City of Boulder Forestry 2021; Denver Parks and Recreation 2018; Nowak et al. 2010). In Colorado, white ash trees are planted along residential areas and are a valuable part of urban tree canopies. White and green ash (*Fraxinus pennsylvanica*) trees together make up over 15% of urban forests in Colorado (Colorado Dept of Agriculture 2021).There were no visible signs of pest infestation or damaged wood on our focal trees during the study period.

The study site was situated at the University of Colorado Boulder East Campus (40.011132, -105.242205; 1655 meters; Figs. 1a,b). The climate is temperate with an average high temperature of 26.9 ºC in July, and average low temperature of -7.8 ºC in February (NOAA). During 2018, average daily wind speeds ranged from 0 to 4.5 meters/second spanning

all cardinal directions (Skywatch Weather Archive 2018). Peak gusts were observed between 15.6 to 33.5 meters/second, predominantly from the west (Skywatch Weather Archive 2018). The focal ash trees were part of a row of eight white ash trees planted in 1991 in a turfgrass plain two meters west of a sidewalk (Fig. 1c). These focal trees were eight meters apart, did not have overlapping canopies, and were referred to as Tree1 and Tree2 (Fig. 1c). There was a second row of white ash trees on the east side of the sidewalk. To the north, there was a mixed conifer-deciduous wetland. A fenced meteorological station (550 square meters) was seven meters to the southwest of the trees and a three-story university building was approximately 50 meters southwest of the trees. Within the meteorological station, a north-facing time-lapse camera was mounted on a post four meters above the ground. The camera was 24 meters from Tree1 with canopies of both focal trees in the field of view. The diameters at breast height were 28 cm and 25 cm and heights were 7.8 and 7.4 meters for Tree1 and Tree2, respectively.

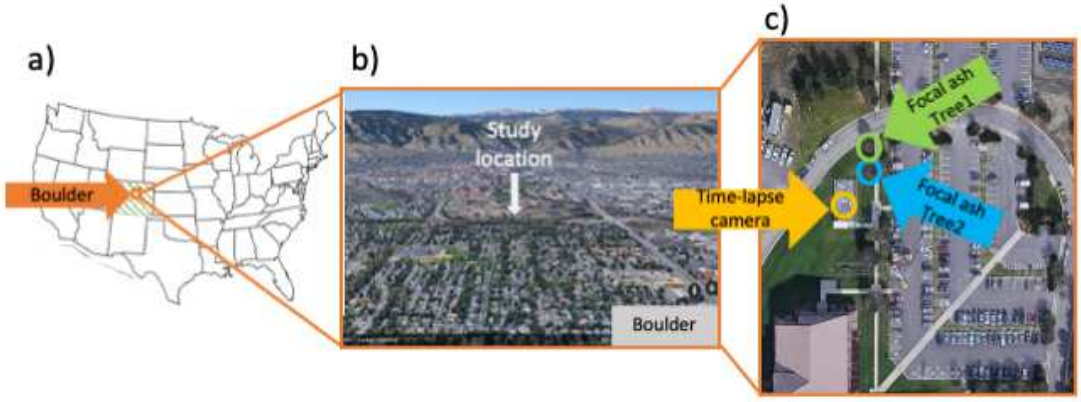

Figure 1. a) Map highlighting study location in Boulder, CO. b) Aerial image showing urban landscape of Boulder, CO (Google Earth 2021). c) Aerial image shows location of focal ash trees and the time-lapse camera (Google Earth 2021).

2.2. Tree motion: theory, measurements and data processing

201 *2.2.1. Accelerometer-derived tree sway theory*

202

203 Tree phenology was inferred using tree sway frequency and periods derived from multi-
204 axis accelerometers. The frequency of vibrations, or sway cycles, is inversely related to the
205 tree's mass and the period of a sway cycle is proportional to the mass (Moore and Maguire
206 2004). *Equation* (1) shows this relationship conceptually,

207 $$f_0 \propto \sqrt{k/mb} \iff DP \propto \sqrt{mb/k} \quad (1)$$

208 where f_0 is the dominant resonant frequency (Hz), k is a measure of stiffness, m is mass, b is a
209 measure of damping, or the decrease in the amplitude of oscillation as energy is lost from the
210 system, and DP is the dominant period in seconds (Moore and Maguire 2004).

211 In this paper we focused on accelerometer data displayed as the dominant period (DP),
212 or the time in seconds for the tree to complete one cycle of sway. Over the course of a growing
213 season, a deciduous tree's aboveground mass increases with leaf emergence and decreases
214 with leaf drop. A temporary increase in mass is detected as a corresponding temporary increase
215 in tree sway period (see Equation 1). Estimating the actual tree mass is not needed since we
216 are using the dominant resonance period as a proxy measure for the relative percent change of
217 mass, which should change with spring and autumn phenology or other events that alter a tree's
218 mass (Gougherty et al. 2018; Baker 1997). Similarly, although sufficient wind is necessary to set
219 the tree in motion (van Emmerick et al. 2017), estimating wind speeds is not necessary to
220 determine the dominant period. When wind is below the threshold for initiating tree motion, the
221 accelerometer is recording "noise" and tree sway period cannot be identified in these cases.

222 It is important to recognize that the tree sway period is linked to mass changes on both
223 the inside and outside of the tree. In our study, we are interested in multi-day or week trends of
224 seasonal growth and the associated biomass changes related to foliage gain or loss and
225 vascular transport. The tree's mass may also change with episodic events such as precipitation

or structural damage. In the case of precipitation, rainfall interception on foliage or branches may increase the mass and lengthen the dominant period during the rain event for minutes to days (van Emmerik et al. 2017). Mass loading from snowfall might show more pronounced fluctuations in dominant periods depending on the snow water content and time to melt (Raleigh et al., 2021). These episodic mass loading events are likely captured in our data but are not expected to contribute to the overall seasonal signal.

While we expect tree mass to be the strongest determinant of tree sway periods, several other tree properties such as stiffness, wood density, and canopy architecture also have an effect (Moore and Maguire 2004). The growth and hardening of xylem changes trunk diameter and the stiffness of a tree over its lifetime (Bunce et al. 2019); however, stiffness is not expected to have significant influence within an annual phenology signal (De Langre 2019). Seasonally, the hydraulic conductance of water up the stem changes, affecting the stiffness (Ciruzzi and Loheide 2019; van Emmerick et al. 2017). As water and sap move through the tree tissue the trunk vibrations may be affected due to changes in the trunk stiffness and therefore confounded with the mass; however, the seasonal change in stiffness is considered of secondary importance to the seasonal change in mass when observing across the growing season (Gougherty et al. 2018; van Emmerick et al. 2017). The canopy architecture and branching structure of deciduous trees can also affect the stiffness and damping of tree movement (Schindler et al. 2013). The natural or pruned structure could explain differences in dominant period when comparing among trees; therefore, we selected two white ash trees that have similar canopy architecture and branching patterns and were not pruned over the study period. Stiffness was not measured (i.e., with a bending test) as these trees were the same species and close enough in size and age to assume similar stiffness.

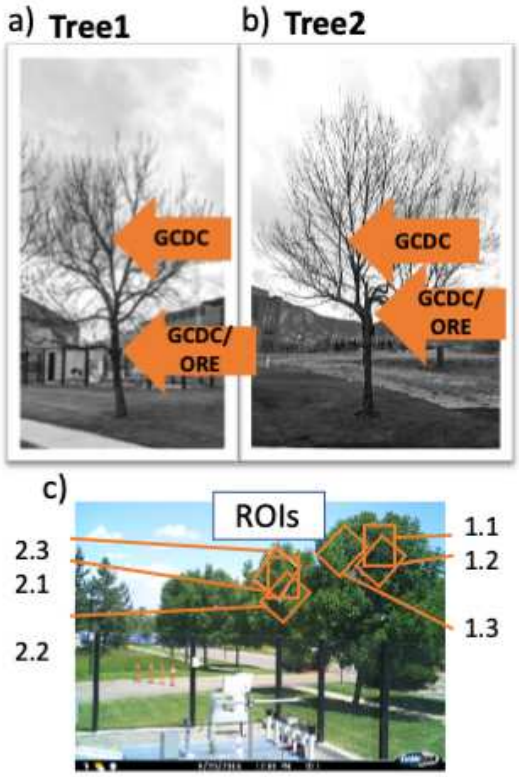

Figure 2. Diagrams of accelerometer position and height for ORE and GCDC accelerometers on a) Tree1 and b) Tree2. Panel c) shows regions of interest for Green Chromatic Coordinate analysis of time-lapse imagery on Tree1 (1.1 - 1.3) and Tree2 (2.1 - 2.3).

2.2.2. Device positioning and power

A total of six accelerometer units of three types were tested between 2018-2020 (n=4 model X16-1D, Gulf Coast Data Concepts [GCDC], Waveland, MS; n=1 model AL100, Oregon Research Electronics [ORE], Tangent, OR; n=1 model AL100-solar, ORE) (Fig.2). Only data from 2018 are presented since that dataset was the most complete. Accelerometers were installed March 23rd, 2018. An ORE (AL 100 on Tree1, AL100-solar on Tree2) and a GCDC unit were placed at the start of crown branching from the main trunks of each tree at a height of 2.1

meters above the ground (Figs. 2a,b) with the x-axis oriented vertically to the tree trunk. These GCDC units will be referred to as the lower at-crown GCDC units. Separate GCDC units were also placed on a vertical secondary branch above the crown branching at 3.7 and 2.8 meters above the ground, also with the x-axes oriented vertically, representing the upper above-crown units of Tree1 (Fig. 2a) and Tree2 (Fig. 2b), respectively.

The ORE and GCDC units logged acceleration on two perpendicular, lateral planes (north-south or east-west for the y- and z-axes) and one vertical direction (x-axis) that is a measure of the acceleration of gravity. ORE units were positioned on the eastward side of the tree with the y-axis oriented north-south and the z-axis oriented east-west (ORE Manual page 10, 2020). The GCDC units were positioned on the northward side of the tree with the y-axis oriented east-west and the z-axis oriented north-south (GCDC Manual page 7, 2022). Because we positioned the at-crown units on perpendicular sides of the tree, the y- and z- axes of the GCDC and ORE were oppositely aligned. The x-axis on the plane parallel to the tree trunk was excluded from analysis and served to confirm the accelerometer is functioning as expected.

We prepared GCDC and the ORE units for long term deployment and checked and replaced batteries every three to four months. We used polyvinyl bags and electrical tape to form a weatherproof barrier around the GCDC accelerometers. ORE hardware was already waterproofed. The GCDC units were manufactured to operate on a single AA battery cell. Preliminary testing showed the AA battery powered a GCDC unit logged continuously at 12 Hz for an average of 25.6 days. Therefore, in an attempt to improve longevity we engineered the GCDC units to receive power from four D-cell batteries oriented in parallel. The ORE AL100 unit was manufactured to operate on two C-cell batteries. The ORE AL100-solar unit on Tree2 was engineered by the manufacturer to use solar power and stored in a rechargeable C-cell battery.

2.2.3. Device programming

288 ORE accelerometers logged the XYZ axes continuously at a sample rate of 10 Hz,
289 resulting in 864,000 samples per day collected in one comma-separated values (csv) file per 24
290 hours. At the start of study, it was not clear that we could have changed the ORE sensor to
291 sample at 12 Hz to align with the GCDC sensors. Although we later discovered this was
292 possible, we do not believe the difference in sample rate of this magnitude significantly affected
293 results since accelerometers, GCDC in particular, can fluctuate by about 1 Hz from a set
294 frequency (Evans et al. 2014). GCDC accelerometers logged the XYZ spatial axes dimensions
295 continuously at a sample rate of 12 Hz, resulting in 1,036,800 samples per day collected in
296 seven to eight csv files per day. The GCDC configuration options ranged from 12 to 800 Hz, and
297 so 12 Hz was selected to most closely align with the ORE sensors.
298
299 *2.2.4. Data processing and statistical analysis*
300
301 Raw acceleration data from the two lateral axes were converted to phenological
302 estimates. The data processing followed three steps defined by Gougherty et al. 2018: 1)
303 identify DPs, 2) remove outliers, and 3) fit a phenology model to estimate the onset dates of
304 spring, autumn and the growing season length.
305 In step one, the spectral density, which shows the strength of variation as a function of
306 frequency, was estimated using an autoregressive model to minimize Akaike Information
307 Criterion. For each sensor's y and z-axis, separate periodograms were generated from the
308 spectral density with the 'ar' and 'spec.ar' functions in the *stats* package of R (R Core Team,
309 2019). Peaks in the periodograms were found with the 'findpeaks' function in the *pracma*
310 package (Borchers, 2019). The dominant and second-most-dominant periods were calculated
311 as 1/frequency of the peaks with the highest and second highest spectral density, respectively.
312 Each dominant period (DP) was assigned a weight based on the difference between the
313 spectral density of the most and second-most dominant period identified in the periodogram for

a given day of year. The DPs and associated weights of both axes were combined into one dataset; meaning for each 24-hour period, a DP and the associated weight from the y- and z-axes were represented in an interleaved time-series. In step two, outliers less than 0.9 seconds and greater than 3.0 seconds were manually removed from the ORE and GCDC datasets. The limits were selected based on visual inspection, and also on typical sway periods documented for trees of similar size. We note that the typical range of sway period will depend on tree species, height, age, and other variables (Jackson et al. 2021), and the values used here are specific to the study trees. The remaining outliers were removed using a locally weighted regression (LOESS curve; Cleveland and Devlin 1988) that removed data points with residuals greater than the threshold of 1.5 times the interquartile range. In step three, a dual-logistic curve was used to model the full growing season (Elmore et al. 2012; Eq. 2).

$$DP = m_1 + (m_2 - m_7 \cdot t) \cdot (1/(1 + e^{\frac{m_3 - t}{m_4}}) - 1/(1 + e^{\frac{m_5 - t}{m_6}})) \quad (2)$$

In *Eq.* (2), *DP* represents the dominant period, *t* is the day of year, m_1 is the DP during dormancy, m_2 is the difference in DP during dormancy versus active growth, m_3 and m_4 influence the shape of the logistic curve in the green-up, m_5 and m_6 influence the shape of the logistic curve during senescence, and m_7 changes the slope of the curve during the summer. The m_3 parameter indicates the spring inflection point, or the date at which the DP during the early season is changing the fastest, which we used to represent the start of spring (SOS). The m_5 parameter indicates the autumn inflection point, or the date at which the DP during the end of the season is changing the fastest, which we used to represent the start of autumn (SOA). In instances where there were missing data for SOA due to battery failure, SOS could still be accurately modeled by temporarily using estimated data to fill the autumn gap. The length of season (LOS) is the difference in number of days between SOS and SOA.

The peak flowering (PF) date was determined by identifying the date at which the dominant period (DP) was highest (i.e., the maximum DP value) before SOS. Days were

339 averaged to find the PF if multiple max DPs were found. Unit and height comparisons of the
340 mean DP values per day were performed using Student's t-tests and Pearson's correlation tests
341 across Julian days 82 to 270 during 2018, which had complete data across all six
342 accelerometers.
343
344 *2.3. Time-lapse photography analysis*
345
346 We used RGB brightness values from digital camera imagery to calculate green
347 chromatic coordinates (GCC) from Red-Green-Blue (RGB) digital numbers (GCC = Green/[Red
348 + Green + Blue]). A north-facing, 20-megapixel Cuddeback trail camera (model ELCA 1224,
349 Cuddeback Digital, De Pere, WI) photographed the two study trees beginning March 27, 2018.
350 The camera was set to record images at 30-minute intervals during the daytime as suggested
351 by Sonnentag et al. (2012), resulting in 19-30 images per day. Single photo dimensions were
352 2576 x 1496 megapixels. Images were analyzed using the *Phenopix V 2.0* package in R
353 according to the phenopix vignette (Filippa et al. 2020). Three region-of-interest (ROI) polygons
354 were each drawn in the canopy of Tree1 and Tree2 (Fig. 2c). Vegetation indices were
355 calculated using a pixel-based analysis where raw color digital numbers were extracted from
356 pixels. The GCCs were averaged over a 3-day moving window in the ROI according to
357 Sonnentag et al. (2012). The same dual-logistic curve used in the accelerometer DP analysis
358 was fit to the data according to Eq. 2 (Elmore et al. 2012). As with the accelerometer analysis,
359 we applied the "derivatives" method (Klosterman et al. 2014), which uses the inflection points on
360 the dual-logistic model curve to define SOS and SOA.
361
362 *2.4. Visual observations*
363

Tree1 and Tree2 were visited approximately one to two times per month between March and December 2018 to record visual observations of phenophases set forth by the National Phenological Network (NPN) in the Phenophase Handbook by Haggerty and Mazer (2008, S3). The phenophases surveyed for in the field were pollen release, full pollen release, emerging leaves, unfolded leaves, ≥ 75% of full leaf size, 50% of leaves colored, all leaves colored, ≥ 50% of leaves fallen, and all leaves fallen. In addition to field observations, time-lapse imagery was visually reviewed to make approximate estimates of phenophases that were not directly observed in the field.

2.5. Phenological method comparison

For accelerometer and time-lapse comparison, SOS, SOA dates and LOS number of days were compared between accelerometer values averaged across sensors on a tree and time-lapse camera values averaged across ROIs on a tree. To determine the difference in days, the mean SOS and SOA dates and LOS days for accelerometers was subtracted from the corresponding time-lapse camera values. To compare visual observations with accelerometer and time-lapse cameras, dates of visual observation of NPN phenophases averaged across Tree1 and Tree2 were compared to the SOS and SOA values averaged with across all accelerometer sensors (on both trees) and across all time-lapse camera imagery ROIs (on both trees). To determine the difference in days, the mean accelerometer and time-lapse camera SOS and SOA dates and LOS days were subtracted from the corresponding mean visual observation dates and days.

3. Results

389 *3.1 Urban tree growing seasons*

390

391 All six accelerometers mounted on the two focal ash trees detected growing season
392 signals in an urban setting, including a progression of flowering. We obtained a precise estimate
393 of PF and were able to model SOS and SOA from the sensors with complete or near-complete
394 data (Fig. 3). Two of the four GCDC sensors had unexpected battery failure in the autumn
395 resulting in the inability to model SOA and LOS for the upper sensor of Tree1 (Fig. 3a) and
396 lower sensor of Tree2 (Fig. 3f). Accelerometer PF, SOS, and SOA had low variation within and
397 between trees, on the order of fewer than three days (Table 1).

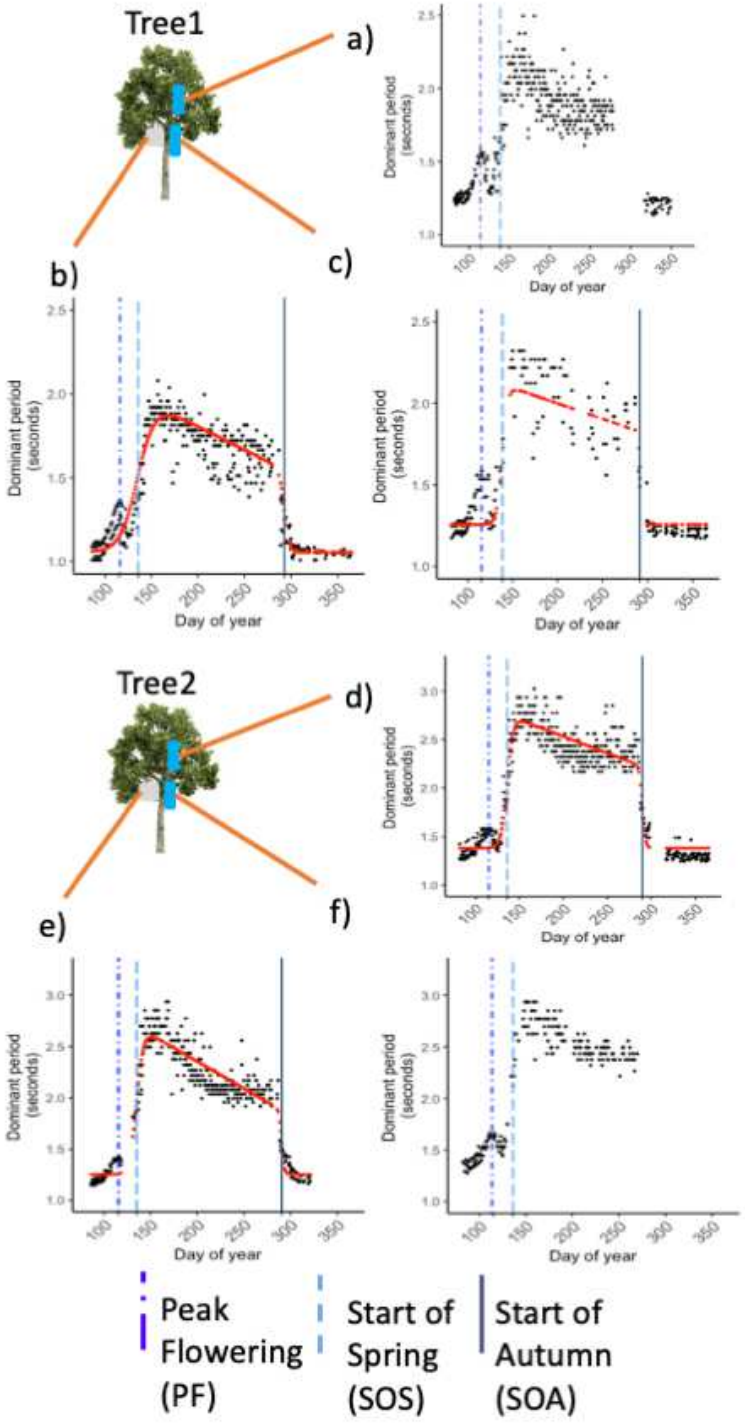
Tree1
a)
b)
c)
Tree2
d)
e)
f)
Dominant period (seconds)
Day of year
Peak Flowering (PF)
Start of Spring (SOS)
Start of Autumn (SOA)

398

399 Figure 3. Time-series of accelerometer dominant period (DP) of y- and z- axes during the 2018
400 growing season for Tree1 (a-c) and Tree2 (d-f). Rectangles on the tree diagram represent
401 accelerometer locations: GCDC (blue) and ORE (gray). DP output is displayed for GCDC-upper
402 in a) and d), ORE in b) and e) and GCDC-lower in c) and f). Vertical lines show the flowering
403 peak (FP; dashed-dotted), model-predicted start of spring (SOS; dashed) and model-predicted
404 start of autumn (SOA; solid).
405
406 *3.2 Time-lapse, visual observations, and accelerometer method comparison*
407
408 Compared to time-lapse GCC, accelerometers showed delayed SOS, delayed SOA, and
409 longer LOS. For LOS, the accelerometer DP was on average 10 days longer than camera-
410 derived measures for Tree1 and 9 days longer for Tree2 (Table 1). For SOS, accelerometers
411 showed more within-tree variation in average dates compared to time-lapse cameras (Table 1,
412 Fig. 4). Accelerometer DP SOS lagged on average 4 and 3 days behind time-lapse GCC for
413 Tree1 and Tree2, respectively. For SOA, accelerometers showed similar within-tree variation in
414 average dates compared to time-lapse cameras for both trees (Table 1). The accelerometer DP
415 SOA lagged behind the time-lapse GCC 13 and 14 days for Trees 1 and 2, respectively.

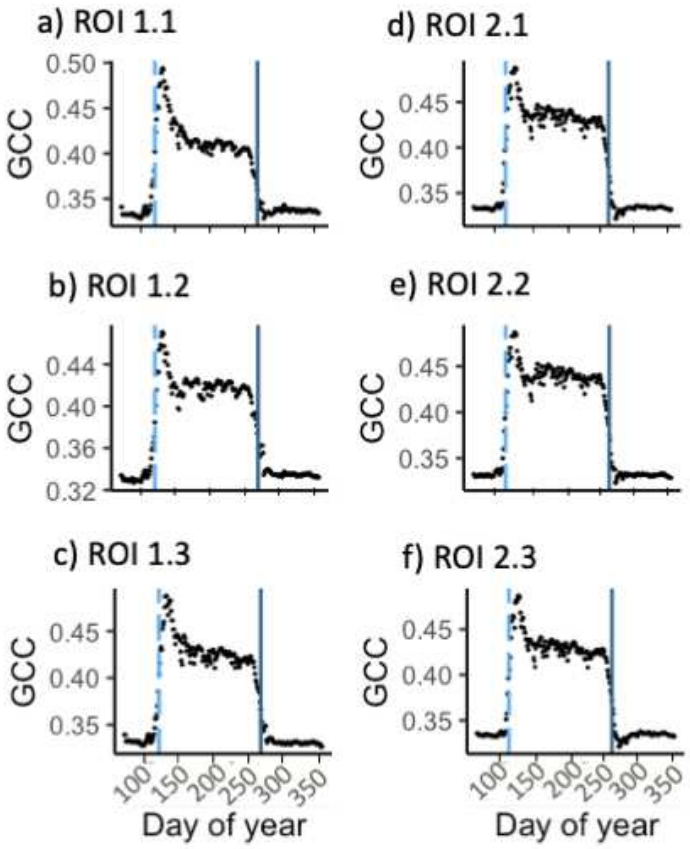

Figure 4. Growing season for 2018 as calculated from green chromatic coordinate (GCC) analysis of image regions of interest (ROIs) (Fig. 2) from time-lapse camera imagery for Tree1 (a-c) and Tree2 (d-f). ROIs 1.1, 1.2, 1.3 capture the canopy of Tree1, and ROIs 2.1, 2.2, 2.3 capture the canopy on Tree2. Vertical lines show model-predicted start of spring (SOS; dashed) and model-predicted start of autumn (SOA; solid) based on the GCC.

Table 1. Average vegetation indices (PF, SOS, SOA, LOS) and standard deviations in parentheses. Accelerometer DP values from the ORE, at-crown GCDC, and above-crown GCDC sensors and GCC values from the time-lapse camera ROIs have been averaged for each tree.

Metric	Tree	Mean PF (day of year)	Mean SOS (day of year)	Mean SOA (day of year)	Mean LOS (number of days)
Accelerometer DP	1	115.2 (+/- 1.0)	138.0 (+/- 1.4)	292.1 (+/-1.5)	154.9 (+/-3.2)
Time-lapse GCC	1	NA	134.0 (+/-1.0)	279.3 (+/-0.8)	145.0 (+/-1.0)
Difference DP-GCC	1	NA	4.0 days	12.8 days	9.9 days
Accelerometer DP	2	114.7 (+/- 1.1)	134.2 (+/- 2.6)	291.0 (+/-0.7)	154.8 (+/-1.5)
Time-lapse GCC	2	NA	131.0 (+/-0)	277.3 (+/-0.6)	146.0 (+/-0)
Difference DP-GCC	2	NA	3.2 days	13.7 days	8.8 days

We estimated which visual observations of phenophases (S3) best align with accelerometer DP and time-lapse GCC-derived SOS and SOA dates (Table 2). The NPN phenophase for deciduous trees that most closely aligned with model-derived metrics of SOS was ≥ *75 % of full leaf size* (or ≥ 75% of full canopy) for accelerometers and *unfolding leaves* for time-lapse imagery (Fig. S4.2). For SOA, the NPN phenophase that most closely aligned to model-derived metrics of SOA was *all leaves colored* for accelerometers and ≥ *50% of leaves colored* for time-lapse imagery (Fig. S4.3).

Table 2. Comparison of visually observed phenophases to accelerometer- and time-lapse camera-derived vegetation indices with standard deviations (in parentheses) for Tree1 and Tree2 combined

Index	NPN Phenophase for deciduous trees	Visual observation (day of year)	Accelerometer mean difference from visual	Time-lapse mean difference from visual observation

			observation (number of days)	(number of days)
PF	Pollen release	113	2.0 (+/- 1.0)*	NA
SOS	Unfolding leaves	128	8.0 (+/- 2.7)	4.7 (+/- 1.9)*
SOS	≥ 75% of full leaf size (or ≥ 75% of full canopy)	139	-3.1 (+/- 2.7)*	-6.3 (+/- 1.9)
SOA	≥ 50% of leaves colored	280.5	10.8 (+/- 1.3)	-2.2 (+/- 1.2)*
SOA	All leaves colored	286.5	4.8(+/- 1.3)*	-8.2 (+/- 1.2)

*Indicates which NPN phenophase was closest to accelerometer or time-lapse- derived SOS or SOA

3.3 Accelerometer-derived flowering peaks

Accelerometer data showed a small peak in DP (around day 115) before the SOS date (Fig. 3) that corresponded with the time at which flowers were visually observed in the field as fully emerged but not yet releasing pollen (day 113, Fig. S4.1c). Manual review of time-lapse camera imagery and meteorological datasets showed no sustained precipitation events over that time-period. Thus, we are confident that the peak in DP before SOS was a flowering peak that started about one month before the main spring green flush, and this was found in the data of all six sensors. Based on visual observations, flower buds were dormant on day 82 and began to swell on day 86. On day 113 inflorescences were fully emerged from floral bud casing with individual flowers still closed. Photos of the tree buds on these dates are supplied in S4. On days 115 and 114, accelerometers recorded maximum DP for Tree1 and Tree2 (Table 1). The

National Phenological Network phenophases that most aligned with this time was open flowers and pollen release.

3.4 Unit and sensor height comparison

The ORE sensor predicted later dates for PF, SOA and LOS, and both later and earlier SOS dates depending on the tree. The estimates for PF, SOS, SOA, LOS collectively varied from 0.5 to 4.5 days between the ORE and GCDC sensors (See Table S1 for each metric). The mean DP across the 2018 growing season for GCDC versus ORE units were significantly correlated in both axes for both trees (Fig. S1). The 2018 mean DP values for GCDC were significantly higher compared to ORE on one lateral plane for both trees (Table S1). For Tree1, the GCDC z-axis 2018 mean DP was 0.2 seconds longer compared to the ORE model y-axis ($t(107.5) = 2.5$, $p = 0.01$). For Tree2, the GCDC z-axis 2018 mean DP was 0.2 seconds longer compared to the ORE model y-axis ($t(210.7) = 2.3$, $p = 0.01$). The 2018 mean DP was not significantly different between GCDC y-axes and ORE z-axes. The C-cell battery powered ORE sensor consistently maintained power for 90-120 days between battery checks. The four continuously logging GCDC units with D-cell batteries remained powered for an average of 88.5 days during year 1, 28.3 days during year 2, and 15.3 days during year 3. The ORE AL100-solar unit held power for an average of 114 days between our checks from March-November 2018. With decreasing daylight, it appeared that the solar power supply was not strong enough to power the unit in the winter and we ceased field testing after 2018.

The upper above-crown GCDC sensors predicted similar PF dates and SOS dates compared to the lower, at-crown GCDC sensors. The upper position GCDC sensors were 1.5 days earlier and 1.7 days later for PF for Tree1 and Tree2, respectively, and 0.2 and 4.9 days later for SOS for Tree1 and Tree2, respectively, compared to the lower position (Table S2). SOA and LOS values could not be compared between sensor heights due to missing data. The

mean 2018 DP for GCDC upper and lower position units were significantly correlated in both axes for both trees (Fig. S2). The mean 2018 DP values on the y-axes of the lower, at-crown sensor on Tree1 were 0.2 seconds shorter compared to the upper, above-crown sensor ($t(224.8)= -3.7$, $p <0.001$); however, the z-axes showed no difference (Table S2). For Tree2 there was no significant difference in mean 2018 DP between the upper and lower GCDC sensors for either axis.

4. Discussion

Our study demonstrates growing season transitions can be detected in individual trees within an urbanized landscape using trunk-mounted accelerometers. Before SOS and complete spring green-up, our accelerometers detected mass changes associated with flower emergence on the white ash trees. To our knowledge, this is the first observation of tree flowering from DP analysis of acceleration data. This sensor-based approach to monitoring individual trees has promise in capturing vegetation changes that are not typically extracted from imagery-based analyses. Our study provides a launchpad for future studies using accelerometers to incorporate floral observation into hypotheses, include floral phenophases in growing-season models, and create an automated processing platform so accelerometers can serve as inexpensive “Fitbits” (individual activity trackers) for trees. If we consider the accelerometer-derived phenology outcomes observed across the growing season (Figs 3 and 4), the change in accelerometer DP resembles an NDVI growing season curve typical of a deciduous tree (e.g. Motohka et al. 2010). Although, beginning in mid-summer there is a more prolonged and gradual decrease in sway period than the typical late-summer decline of NDVI, suggesting accelerometers may provide more detailed insight into water loss during dry periods or autumn foliage changes. While we only included two trees in this study, the consistency between multiple sensors on the trees provides evidence for a strong pattern despite the sample size.

508 Contrary to suggestions by Gougherty et al. (2018), the current study provides evidence
509 that trees do not need to be located on the city edge or open, exurban areas to obtain a wind-
510 induced phenological signal. Many urban trees are adjacent to buildings and houses, linearly
511 planted along sidewalks, medians, and property edges to provide shade or delimit boundaries.
512 Outside of parks or natural spaces, there is infrequently a distinct forest edge within the urban
513 matrix. Our data suggest, however, that wind-blocking buildings and adjacent trees do not
514 hinder ability to obtain a phenological signal from urban trees. More research is needed to
515 determine if there are thresholds or optimums in building distance, composition, and density that
516 may affect the amount of wind necessary to induce tree motion measurable with
517 accelerometers.
518
519 *4.1. Method comparison*
520
521 The discrepancy between accelerometers, time-lapse cameras, and visual observations
522 are not surprising since the tools measure different tree attributes (i.e., motion/mass, greenness,
523 and categorical assessment, respectively); nonetheless, our results suggest that
524 accelerometers may offer a robust method for consistent detection of SOS and SOA. It was
525 surprising that the accelerometer-based estimate of SOS did not align to visually observed *leaf*
526 *unfolding* as was found with past SOS dates of Balsam poplar (Gougherty et al. 2018),
527 suggesting that accelerometer comparison to NPN visual phenophases for deciduous trees may
528 depend on the species. SOA also was earlier by nearly two weeks for time-lapse camera-
529 derived dates compared to accelerometers for both trees (Table 1). Past research shows that
530 there are more challenges associated with measuring SOA than SOS when using time-lapse
531 GCC, since loss of chlorophyll is more gradual in autumn than the gain in spring and because
532 leaf coloring and leaf drop phenophases may overlap (Elmore et al. 2016; Klosterman et al.
533 2014; Elmore et al. 2012; Ganguly et al. 2010). While past study comparisons between

534 accelerometer SOA and leaf drop were not correlated (Gougherty et al. 2018), our study
535 suggests the accelerometer SOA values may be more related to senescence (Table 2). While
536 SOS and SOA estimates were fairly consistent between accelerometer units on a given tree,
537 conducting visual observations using a more detailed set of phenophases with increased
538 observation intervals may serve to capture greater precision in linking phenophases from the
539 globally-used BBCH scale (Finn et al. 2007) or those described in the National Phenological
540 Plant Profiles (National Phenology Network 2008) to accelerometer model parameters.
541 The alignment of the accelerometer-derived and image-based SOA and SOS estimates
542 with different NPN phenophase observations suggests that these tools may provide
543 complementary information that could constitute a more complete, high-resolution picture of tree
544 phenology. The seasonal onset dates derived from accelerometers could be leveraged as a tool
545 to fill niches not captured in near-surface and satellite-based phenological observation. First, the
546 accelerometers detected flowering phenophases that were not captured by the time-lapse photo
547 analysis. Second, compared with time-lapse GCC, we found accelerometer DP aligned with
548 different observer-based phenophases of SOS and SOA. This outcome suggests
549 accelerometers may better serve to complement rather than validate time-lapse imagery. If the
550 accelerometer lag in seasonal onset dates compared to time-lapse cameras proves to be
551 widespread and consistent within ash trees or for other tree species, *paired* accelerometer and
552 time-lapse camera data would be valuable to generate a more comprehensive picture of tree
553 phenology. This dual-instrument approach may be particularly useful for measuring autumn
554 phenophases involving both color and mass changes (e.g., senescence and leaf drop and
555 potential overlap) and temporal information about flowering phenophases that are not captured
556 by imagery.
557
558 *4.2. Floral phenology*
559

560 Extracting the dates from mass changes associated with flowering such as start, peak,
561 end and length of flowering would be important contributions to instrument-based phenology
562 monitoring. Our data shows flowering time can be clearly observed for ash (*Fraxinus*) tree
563 species that produce wind-pollinated flowers before spring leaf flush (Fig. 3) and supports use of
564 accelerometers for date extraction from other species that flower before full foliage. We
565 considered other explanations for this peak due to external loading factors such as prolonged
566 snow interception followed by unloading or any other precipitation events. Precipitation events
567 could increase the DP due to added water mass on the tree, but this is not a plausible
568 explanation because the timescale of such spring-time events (hours to days) is considerably
569 shorter than the duration observed for the DP rise and fall (approximately 30 days).
570 There are many challenges associated with using imagery to determine flowering
571 phenophases for species. First date of flowering in corn fields has recently been detected using
572 multispectral reflectance data from satellites (MODIS and Sentinel-2; Nguyen et al. 2018);
573 however, extension of this method to mixed-species areas is limited by spatial resolution. For
574 digital repeat photography, there is some limited evidence of detection of flowers on individual
575 trees. RGB brightness and saturation levels may have different ratios when comparing
576 individual trees with flowers to individuals without flowers (Sturm et al. 2018). Kim et. al (2020)
577 employed machine learning techniques to identify presence or absence of flowering events in
578 trees with concentrated white blossoms using high-resolution digital cameras; however, the
579 authors suggest that the imagery collections from phenological networks focused on leaf
580 phenology (e.g., National PhenoCam Network) likely do not have sufficient pixel resolution for
581 assessing the complex reflectance patterns of flowers. Phenology camera analyses can count
582 the number of flowers at peak bloom on individual trees in digital images (Crimmins and
583 Crimmins 2008; Adamsen et al. 2000); however, they have not accurately detected the timing of
584 flowering phenophases (Sunoj et. al, 2016). While accelerometers also track on an individual
585 tree basis, they offer the advantage of using mass changes to learn about floral development

586 over time (and potentially relative quantity) regardless of flower colors, blossom size, pixel
587 resolution, and obstructions from neighboring foliage or light, which can hinder widespread use
588 of imagery for study of flowers.
589 A simple, inexpensive sensor-based approach to track flowering could revolutionize
590 efficiency in the urban forestry and agricultural sectors. Estimated flowering dates delivered to
591 land managers and orchardists in real-time from accelerometers could contribute to enhanced
592 understanding of crop development, frost or floral damage, as well as generating harvest
593 predictions or maintenance schedules in response to weather conditions that vary annually.
594 Microclimates can have a strong effect on plants even within the same orchard (Verdugo-
595 Vásquez 2016) or city block (Ziter et al. 2019; Chen et al. 2018; Bonan 2000). Predicting tree
596 flowering time could improve the efficacy of arboreal operations such as timing when to apply
597 nutrients or administer disease interventions (Pusey and Curry 2007). Using accelerometers to
598 create a phenology network in the agricultural and urban forestry sectors could improve
599 efficiency of tree maintenance with potential to enhance crop yield or tree survival. Thus,
600 accelerometers show great potential as an objective and automated method to detect flowering
601 phenophases that are not typically captured with other instrument-based measurements.
602
603 *4.3. Unit type and placement characteristics*
604
605 Our results provide evidence that data from multiple types of accelerometers within or
606 across tree studies may be suitable for direct comparisons of phenological dates when placed at
607 the same trunk height. The three-day variation of PF, SOS, and SOA estimates for unit types
608 (Table S1) may be similar to variation found among typical monitoring field visits spanning days
609 to weeks in frequency (Richardson et al. 2018; Elmore et al. 2016). For only the y-axes, the
610 ORE models showed lower DP values for estimated foliage transitions (Fig. S1) suggesting
611 there may be more detailed information gained from analyzing both lateral axes. Weather

612 proofing, long-term battery power, and simple and consistent data transfer were the
613 accelerometer properties that were most important to longevity and ease of use in our study.
614 We found that simple polyvinyl plastic bags and electrical tape, as we used with the GCDC
615 units, were sufficient waterproofing for at least three years of field use. Despite adding the four
616 D-cell batteries, the biggest obstacle in using the GCDC sensors was decreasing battery run
617 times, which was especially prevalent beyond one year of use in a variety of weather conditions.
618 Other power mechanisms such as line power or rechargeable batteries with solar panels may
619 be more successful for multi-year study (Raleigh et al., 2021). Data transfer with an extended
620 universal serial bus (USB) was also slow with GCDC, about 2 hours to download approximately
621 3 gigabytes of data for 3-4 months of sampling using USB connection. The microSD card, as
622 used with the ORE design, was much faster at transferring the daily csv file to a laptop in the
623 field. GCDC software allows a maximum of 999 csv files to be saved before data needs to be
624 downloaded and removed off the microSD card, which could be a hurdle for multi-year data
625 collection without clearing memory. While the more expensive ORE units offer greater ease of
626 use out of the box than GCDC, the similarity of phenological dates extracted between these
627 units suggests that there are opportunities to test other low-cost units that optimize properties
628 such as longevity and ease of use.
629 Accelerometer placement height did not show tradeoffs associated with signal detection
630 and ease of access in an urban environment. Sensors placed higher in the tree have a stronger
631 likelihood of detecting signals due to more movement from wind (van Emmerick et al. 2017).
632 However, the upper secondary branches can have a different signal from the main trunk that
633 may not represent the whole tree (Spatz and Theckes 2013). The sensors we placed above-
634 crown (3.7 and 2.8 from ground) versus at-crown (2.1 meters above ground) resulted in 0.2
635 days difference in SOS for Tree-1 y-axis; no differences were found for Tree1 z-axis and for
636 both axes of Tree2. Our DP analysis supports the idea that at-crown sensor placement is
637 sufficient for detecting PF, SOS and SOA within the urban matrix; the lower device placement

638 on the main trunk had sufficient tree sway for vegetation date detection and reduced likelihood
639 of picking up secondary sway signals that might not represent the whole tree as Gougherty et
640 al. (2018) found with placement at 1 meter from the ground. For many shade-bearing street
641 trees, such as white ash, placing a unit at the base of the crown offers reasonable access with
642 use of a small stepladder, avoiding the need for tree climbing equipment.
643
644 *4.4. Future research*
645
646 Developing an understanding of what structural landscape elements can hinder or help
647 accelerometer use on trees is essential to unlocking population-level studies. Our study
648 demonstrates that accelerometer-derived tree phenology is possible within the urban matrix,
649 and merits continued study of the urban landscape with larger sample sizes. A useful next step
650 would be to see if there are dead zones without sufficient wind to force tree sway. We
651 recommend investigating whether dead zones may be predictable based on above-ground
652 landscape elements, topography, urban morphology and wind flow properties (Cionco and
653 Ellefsen 1998; Ottosen et al. 2019). Because street median and sidewalk trees are often the
654 same age, they offer an opportunity to systematically test different landscape variables such as
655 distances to buildings, building density, or different species of trees. Species-specific life cycle
656 data is valuable for management challenges such as controlling invasions (Maan et al. 2020)
657 and green infrastructure testing such as stormwater retention properties (Houdeschel et al.
658 2015). Continued development of accelerometer-based study of tree species within and across
659 cities may aid in assessing range shifts for urban planting guides.
660 Future work could also target development of phenological models for early flowering
661 species and explore how other reproductive strategies may be modeled from tree sway data.
662 Integration of two dual-logistic curves into a single model for trees that flower before the spring
663 green-up may be appropriate for such species. In the case of wind-pollinated tree species, the

release of pollen may allow for a defined progression of mass changes as modeled by the DP produced by the ash trees in our study. It is still unknown how accelerometer-derived phenology curves may represent flower and leaf emergence in trees that have simultaneous leaf and flower development. Due to genetic variation in tree flowering time within the lifecycle of a species, models may need to be specific to species or functional types (i.e., early- or late-flowering trees) to enable monitoring of tree communities. Exploration of accelerometer-derived tree sway on species that are insect-pollinated would also contribute to a more comprehensive understanding of how flowers and pollen release may be modeled.

Continued testing of other accelerometer units that minimize the tradeoffs between performance and cost will be of value to scaling up the number of trees in a study. Testing of other low-cost accelerometers that have weatherproof designs and improved power systems will be of value for larger, population-level studies. Furthermore, accelerometers with wi-fi enabled transmitting systems would advance the capacity for accelerometers to be more automated, similar to studies of people's mobility patterns in cities using data streams from common devices (Kontokosta and Johnson 2017). For instance, single-board computers (e.g. Raspberry pi) or microcontroller technology (e.g. Arduino) could be used to transmit high-resolution accelerometer data to online servers (Okigbo et al. 2020). This real-time connection could save considerable time for land managers and researchers and enable more responsive management. Additional time savings for phenological monitoring of multiple trees might be further achieved with video monitoring methods, which have been developed to track tree motion in time (Barbacci et al. 2014).

These results have also led to interesting questions about how accelerometers can be used for observing processes influencing mass change beyond seasonality of deciduous trees. The seasonal changes of coniferous trees may be modeled differently from those of deciduous trees (Jackson et al. 2021) and there may be greater potential to capture high temporal resolution information about reproductive phenophases without overlap of the mass changes

associated with foliage. There are many opportunities to explore how tree age, size, architecture, and management may impact the mass and tree sway relationships for phenophases across time. Accelerometers could be useful in identifying disease, locating structural damage, and making field site visits more efficient. For example, Emerald Ash Borer infestations kill branches by slowly severing the vascular tissue (Poland and Mccullough 2006). As branches die, the tree's mass may reach a threshold of change that is detectable by an accelerometer. In the case of a storm, tree biomass could be rapidly reduced following wind or snow damage. If a forester could monitor a pest-infested tree or be notified of structural damage produced by a storm, they may find more efficiency in managing the health of trees and associated ecosystem services. Deriving quantitative changes in biomass (e.g., due to pest damage, or leaf on/off) from changes in tree sway requires additional data and methodological refinements not explored here, such as the stiffness and damping properties of the tree (Equation 1). Additionally, such quantification requires identification of an appropriate functional relationship between sway and biomass, which might be modeled differently (e.g., cantilever versus pendulum approximations) depending on canopy architecture and for broadleaf versus coniferous trees (Jackson et al., 2021).

5. Conclusions

Using accelerometers to determine tree phenology is an emerging frontier in sensor-based ecological research. Our study demonstrates that high-resolution seasonal transitions can be extracted from trunk-mounted accelerometers in an urban environment. Whether in a city or a continuous forest, accelerometers have potential to fill a niche in sensor-based approaches to measuring foliar and reproductive phenology. Furthermore, accelerometers may complement established near-surface remote sensing methods such as digital repeat photography (e.g., PhenoCams) and traditional visual human observations for a more objective

and detailed understanding of tree biology. The low-cost, non-invasive nature of accelerometer-tracked mass changes around flowering time could revolutionize larger-scale study of tree phenology in the urban forestry and agricultural sectors and help identify bioindicators of climate and land use change.

Future work could target understanding landscape controls on signal thresholds, building phenological models for tree flowering time, and testing types of widely available accelerometers that are likely to be successful for practical use in tree phenology studies. Continued development of automated data flows from accelerometers to on-the-go apps for mobile devices opens avenues for efficient use of a rich set of information on tree seasonality, disease, insect infestation, and structural damage. Tree health is vital to many ecological processes and ecosystem services. Accelerometers offer an opportunity for enhanced understanding of how trees across biomes are responding to climate change, regional urbanization, and other localized environmental influences.

Conflicts of interest

The authors declare no conflicts of interests.

Authors' contributions

DJ developed the study design with support from CW, BM, JF and MR. DJ and AL collected data; DJ, AL, and MR conducted analysis; DJ led the manuscript writing with contributions and feedback from all authors.

Acknowledgements

741 The authors thank Dr. Gabriel Senay (EROS data center and North Central Climate Adaptation
742 Center) for advising on the study design and project feedback. We appreciate all the tree
743 climbing to mount, maintain, and remove sensors by arborists Vince Aquino, Joel Serafin,
744 Roland Boler, and Chip Horner (University of Colorado Boulder). We thank Dr. Jim Wagner
745 (Oregon Research Electronics) for providing the AL101 ORE solar unit and for critical technical
746 support. We express gratitude to Alan Scott Kittleman (ATOC Skywatch University of Colorado
747 Boulder) for assistance with the time-lapse camera set-up and Skywatch datastream, Drs. Tim
748 Seastedt and Katharine Suding (University of Colorado Boulder) for advising with project
749 development, Stine Skalmerud for assistance with data collection, and Julia Rothey for editorial
750 support. Thank you to Dr. Paul Cryan (USGS Fort Collins Science Center) and two anonymous
751 reviewers for their thoughtful contributions and suggestions that improved this manuscript. This
752 material is based upon work supported by the National Science Foundation Graduate Research
753 Fellowship Program under Grant No. (1650115) and the Graduate Research Internship Program
754 (GRIP). Any opinions, findings, and conclusions or recommendations expressed in this material
755 are those of the author(s) and do not necessarily reflect the views of the National Science
756 Foundation. Coordination of GRIP at USGS is through the Youth and Education in Science
757 programs within the Office of Science Quality and Integrity. A portion of this research was
758 supported by the U.S. Geological Survey North Central Climate Adaptation Science Center and
759 Fort Collins Science Center. Any use of trade, firm, or product names is for descriptive purposes
760 only and does not imply endorsement by the U.S. Government.
761

762 References

763

764 Adamsen, F. J., Coffelt, T. A., Nelson, J. M., Barnes, E. M., & Rice, R. C. (2000). Method for
765 using images from a color digital camera to estimate flower number. *Crop Sci.,* 40(3),
766 704-709. https://doi.org/10.2135/cropsci2000.403704x

767 Badeck, F.-W., Bondeau, A., Bottcher, K., Doktor, D., Lucht, W., Schaber, J., & Sitch, S. (2004).
768 Responses of spring phenology to climate change. *New Phytologist,* 162(2), 295–309.
769 https://doi.org/10.1111/j.1469-8137.2004.01059.x
770 Baker, C. J. (1997). Measurements of the natural frequencies of trees. *Journal of Experimental*
771 *Botany*, 48(5), 1125–1132. https://doi.org/10.1093/jxb/48.5.1125
772 Bonan, G. B. (2000). The microclimates of a suburban Colorado (USA) landscape and
773 implications for planning and design. *Landscape and Urban Planning*, 49(3), 97–114.
774 https://doi.org/10.1016/S0169-2046(00)00071-2
775 Barbacci, A., Diener, J., Hémon, P., Adam, B., Donès, N., Reveret, L., & Moulia, B. (2014). A
776 robust videogrametric method for the velocimetry of wind-induced motion in trees.
777 Agricultural and Forest Meteorology, 184, 220–229.
778 https://doi.org/10.1016/j.agrformet.2013.10.003
779 Borchers, H.W. (2019). pracma: Practical Numerical Math Functions. R package version 2.2.9.
780 https:// CRAN.R-project.org/package=pracma
781 Bunce, A., Volin, J. C., Miller, D. R., Parent, J., & Rudnicki, M. (2019). Determinants of tree
782 sway frequency in temperate deciduous forests of the Northeast United States.
783 *Agricultural and Forest Meteorology*, 266–267(December 2018), 87–96.
784 https://doi.org/10.1016/j.agrformet.2018.11.020
785 Burroughs, W. J. (2017). Gardening and climate change. *Weather,* 57(5), 151–157.
786 https://doi.org/10.1002/wea.6080570503
787 Cameron, R. W. F., Blanuša, T., Taylor, J. E., Salisbury, A., Halstead, A. J., Henricot, B., &
788 Thompson, K. (2012). The domestic garden – Its contribution to urban green
789 infrastructure. *Urban Forestry & Urban Greening*, 11, 129–137.
790 https://doi.org/10.1016/j.ufug.2012.01.002

Chen, Y., Wang, X., Jiang, B., & Li, L. (2018). The leaf phenophase of deciduous species altered by land pavements. *International Journal of Biometeorology*, 62(6), 949–959. https://doi.org/10.1007/s00484-018-1497-3

Cionco, R. M., & Ellefsen, R. (1998). High resolution urban morphology data for urban wind flow modeling. *Atmospheric Environment*, *32*(1), 7–17. https://doi.org/10.1016/S1352-2310(97)00274-4

Ciruzzi, D. M., & Loheide, S. P. (2019). Monitoring Tree Sway as an Indicator of Water Stress. *Geophysical Research Letters*, 46(21), 12021–12029. https://doi.org/10.1029/2019GL084122

City of Boulder Forestry. (2021). Public Ash Trees Interactive Map. https://boulder.maps.arcgis.com/apps/webappviewer/index.html?id=91f4062312f4491fb9b6465f10fe2066. Accessed Dec 17, 2021.

Cleland, E. E., Chuine, I., Menzel, A., Mooney, H. A., & Schwartz, M. D. (2007). Shifting plant phenology in response to global change. *Trends in Ecology & Evolution*, 22(7), 357–365. https://doi.org/10.1016/j.tree.2007.04.003

Cleveland, W.S., Devlin, S.J., 1988. Locally weighted regression: an approach to regression analysis by local fitting. *J. Am. Stat. Assoc.*, 83, 596–610. https://doi.org/10.2307/2289282.

Colorado Dept of Agriculture. Emerald Ash Borer. (2021) State of Colorado. https://www.colorado.gov/pacific/agplants/emerald-ash-borer

Crimmins, M. A., & Crimmins, T. M. (2008). Monitoring plant phenology using digital repeat photography. *Environ. Manage.,* 41(6), 949- 958. 10.1007/s00267-008-9086-6

Cuddeback Digital. (2014). Cuddeback 20 MP ELCA 1224 camera. https://www.cuddeback.com/shop/Cameras

Denver Parks and Recreation. (May 23, 2018). “The Smart Ash: Denver City Forester- Turned-Superhero Explains Treatment Options to Battle against Emerald Ash Borer (EAB).

https://www.denvergov.org/content/denvergov/en/denver-parks-and-recreation/news/2018/the-smartash--denver-city-forester-turned-superhero--explains-tr.html. Accessed Dec 17, 2021.

DigitalGlobe Inc. (2016) Digitalglobe Atmospheric Compensation (2016) https://www.maxar.com/products

De Langre, E. (2019). Plant vibrations at all scales: A review. *Journal of Experimental Botany*, 70(14), 3521–3531. https://doi.org/10.1093/jxb/erz209

Duraiappah, A. K., Naeem, S., Agardy, T., Ash, N. J., Cooper, H. D., Díaz, S., … Millennium Ecosystem Assessment. (2005). Ecosystems and human well-being: Synthesis. *Ecosystems*, (Vol. 5). https://doi.org/10.1196/annals.1439.003

Elmendorf, S. C., Jones, K. D., Cook, B. I., Diez, J. M., Enquist, C. A. F., Hufft, R. A., … Weltzin, J. F. (2016). The plant phenology monitoring design for the National Ecological Observatory Network. Ecosphere, 7(4). https://doi.org/10.1002/ECS2.1303

Elmore, A.J., Guinn, S.M., Minsley, B.J., Richardson, A.D., (2012.) Landscape controls on the timing of spring, autumn, and growing season length in mid-Atlantic forests. *Glob. Change Biol.*, 18, 656–674. https://doi.org/10.1111/j.1365-2486.2011. 02521.x

Elmore AJ, Stylinski CD, Pradhan K. (2016). Synergistic use of citizen science and remote sensing for continental-scale measurements of forest tree phenology. *Remote Sensing.*, 8. 502; doi:10.3390/rs8060502.

Evans, J. R., Allen, R. M., Chung, A. I., Cochran, E. S., Guy, R., Hellweg, M., & Lawrence, J. F. (2014). Performance of Several Low-Cost Accelerometers. *Seismological Research Letters*, 85(1), 147–158. https://doi.org/10.1785/0220130091

Evans LM, Kaluthota S, Pearce D., Allan GJ, Floate K, Rood SB, Whitham TG. 2016. Bud phenology and growth are subject to divergent selection across a latitudinal gradient in Populus angustifolia and impact adaptation across the distributional range and

associated arthropods. *Ecology and Evolution,* 6: 4565–4581 https://doi.org/10.1002/ece3.2222

Fang F., McNeil, B., Warner, T., Dahle, G., & Eutsler, E. (2020). Street tree health from space? An evaluation using WorldView-3 data and the Washington D.C. Street Tree Spatial Database. *Urban Forestry & Urban Greening*, 49, 126634. https://doi.org/10.1016/J.UFUG.2020.126634

Filippa G., Cremonese, E., Migliavacca, M., Galvagno, M., Folker, M., Richardson, A.D., and Tomelleri, E. (2020). phenopix: Process Digital images of a Vegetation Cover. R package version 2.4. https://CRAN.R-project.org/package=phenopix

Fisher I, Mustard J, Vadeboncoeur M. 2005. Green leaf phenology at Landsat resolution: scaling from the field to the satellite. *Remote Sensing of Environment*, 100, 265-279. 10.1016/j.rse.2005.10.022

Fitchett, J. M., & Raik, K. (2021). Phenological advance of blossoming over the past century in one of the world's largest urban forests, Gauteng City-Region, South Africa. *Urban Forestry & Urban Greening*, 63, 127238. https://doi.org/10.1016/J.UFUG.2021.127238

Fu, Y., Piao, S., Op de Beeck, M., Cong, N., Zhao, H., Zhang, Y., Menzel, A., Janssens, I.A., 2014. Recent spring phenology shifts in western Central Europe based on multi-scale observations. *Glob. Ecol. Biogeogr.,* 23, 1255e1263. 10.1111/geb.12210

Ganguly, S.; Friedl, M.A.; Tan, B.; Zhang, X.; Verma, M. (2010). Land surface phenology from MODIS: Characterization of the collection 5 global land cover dynamics product. *Remote Sens. Environ.*, 2010, 114, 1805–1816. https://doi.org/10.1016/j.rse.2010.04.005

Gérard, M., Vanderplanck, M., Wood, T., & Michez, D. (2020). Global warming and plant–pollinator mismatches. *Emerging Topics in Life Sciences*, 4(1), 77–86. https://doi.org/10.1042/ETLS20190139

867 Gougherty, A. V., Keller, S. R., Kruger, A., Stylinski, C. D., Elmore, A. J., & Fitzpatrick, M. C.
868 (2018). Estimating tree phenology from high frequency tree movement data. *Agricultural*
869 *and Forest Meteorology*, 263(August), 217–224.
870 https://doi.org/10.1016/j.agrformet.2018.08.020
871 Gray, R. E. J., & Ewers, R. M. (2021). Monitoring forest phenology in a changing world. *Forests*,
872 12(3). https://doi.org/10.3390/f12030297
873 Gulf Coast Data Concepts, LLC. http://www.gcdataconcepts.com/products.html
874 GCDC Manual, page 7. (2022). http://www.gcdataconcepts.com/xlr8r-1.html
875 Haggerty, B. P., & Mazer, S. J. (2008). The Phenology Handbook, 43.
876 Hou, Zhang Y, Sun Y, Xu N, Leng Y. 2018. Prediction of firmness and pH for 'Golden Delicious'
877 apple based on elasticity index from modal ana- lysis. *Journal of Food Science,* 83, 661–
878 669.
879 Houdeshel, C. D., Hultine, K. R., Johnson, N. C., & Pomeroy, C. A. (2015). Evaluation of three
880 vegetation treatments in bioretention gardens in a semi-arid climate. *Landscape and*
881 *Urban Planning*, 135, 62–72. https://doi.org/10.1016/j.landurbplan.2014.11.008
882 Hufkens, K., Friedl, M.A., Keenan, T.F., Sonnentag, O., Bailey, A., O' Keefe, J., Richard- son,
883 A.D., 2012. Ecological impacts of a widespread frost event following early spring leaf-
884 out. *Global Change Biol.,* 18, 2365–2377. https://doi.org/10.1111/j.1365-
885 2486.2012.02712.x
886 Iler, A. M., Høye, T. T., Inouye, D. W., & Schmidt, N. M. (2013). Long-term trends mask
887 variation in the direction and magnitude of short-term phenological shifts. *American*
888 *Journal of Botany*, 100(7), 1398–1406. https://doi.org/10.3732/ajb.1200490
889 Inouye, D. W. (2008). Effects of Climate Change on Phenology, Frost Damage, and Floral
890 Abundance of Montane Wildflowers. *Ecology*, 89(2), 353–362.
891 https://doi.org/10.1890/06-2128.1

892 Jackson, T. D., Sethi, S., Dellwik, E., Angelou, N., Bunce, A., van Emmerik, T., Duperat, M.,
893 Ruel, J.-C., Wellpott, A., Van Bloem, S., Achim, A., Kane, B., Ciruzzi, D. M., Loheide II,
894 S. P., James, K., Burcham, D., Moore, J., Schindler, D., Kolbe, S., Wiegmann, K.,
895 Rudnicki, M., Lieffers, V. J., Selker, J., Gougherty, A. V., Newson, T., Koeser, A.,
896 Miesbauer, J., Samelson, R., Wagner, J., Ambrose, A. R., Detter, A., Rust, S., Coomes,
897 D., and Gardiner, B. (2021). The motion of trees in the wind: a data synthesis.
898 *Biogeosciences* 18, 4059–4072. https://doi.org/10.5194/bg-18-4059-2021, 2021
899 Jochner, S., Höfler, J., Beck, I., Göttlein, A., Ankerst, D.P., Traidl-Hoffmann, C., Menzel, A.,
900 2013c. Nutrient status: a missing factor in phenological and pollen research? *J. Exp. Bot.*
901 64 (7), 2081e2092.
902 Kareiva, Peter. Watts, Sean. McDonald, Robert. Boucher, T. (2007). Domesticated Nature:
903 Shaping Landscapes and Ecosystems for Human Welfare. *Science,* 316(5833), 1862–
904 1866. https://doi.org/10.1126/science.1143986
905 Kim, T. K., Kim, S., Won, M., Lim, J.-H., Yoon, S., Jang, K., … Kim, H. S. (2021). Utilizing
906 machine learning for detecting flowering in mid-range digital repeat photography.
907 *Ecological Modelling,* 440, 109419. https://doi.org/10.1016/j.ecolmodel.2020.109419
908 Klosterman, S. T., Hufkens, K., Gray, J. M., Melaas, E., Sonnentag, O., Lavine, I., …
909 Richardson, A. D. (2014). Evaluating remote sensing of deciduous forest phenology at
910 multiple spatial scales using PhenoCam imagery. *Biogeosciences,* 11(16), 4305–4320.
911 https://doi.org/10.5194/bg-11-4305-2014
912 Klosterman, S., Melaas, E., Wang, J., Martinez, A., Frederick, S., O'Keefe, J., … Richardson, A.
913 D. (2018). Fine-scale perspectives on landscape phenology from unmanned aerial
914 vehicle (UAV) photography. *Agricultural and Forest Meteorology*, 248, 397–407.
915 https://doi.org/10.1016/J.AGRFORMET.2017.10.015
916 Korösi, Á., Markó, V., Kovács-Hostyánszki, A., Somay, L., Varga, Á., Elek, Z., … Báldi, A.
917 (2018). Climate-induced phenological shift of apple trees has diverse effects on

pollinators, herbivores and natural enemies. *PeerJ*, 2018(7), 1–21. https://doi.org/10.7717/peerj.5269

Li, F., Song, G., Liujun, Z., Yanan, Z., & Di, L. (2017). Urban vegetation phenology analysis using high spatio-temporal NDVI time series. *Urban Forestry & Urban Greening,* 25, 43–57. https://doi.org/10.1016/J.UFUG.2017.05.001

Lohou, F.; Lopez, A.; Druilhet, A.; Brunet, Y.; Irvine, M.; Lamaud, E. The VENFOR Project: Response of a homogeneous forest canopy to wind stress through the analysis of accelerometer measurements. *In Proceedings of the Wind Effects on Trees*; University of Karlsruhe: Karlsruhe, Germany, 2003; pp. 109–116. hal-02762196

Maan, I., Kaur, A., Singh, H. P., Batish, D. R., & Kohli, R. K. (2020). Evaluating the role of phenology in managing urban invasions: A case study of *Broussonetia papyrifera*. *Urban Forestry and Urban Greening*, 48. https://doi.org/10.1016/j.ufug.2020.126583

Menzel, A. (2002). Phenology: its importance to the global change community. *Climatic Change*, 54, 379–385. https://doi.org/10.1023/A:1016125215496

Moore, J. R., & Maguire, D. A. (2004). Natural sway frequencies and damping ratios of trees: Concepts, review and synthesis of previous studies. *Trees - Structure and Function*, 18(2), 195–203. https://doi.org/10.1007/s00468-003-0295-6

Morisette, J.T., Richardson, A.D., Knapp, A.K., Fisher, J.I., Graham, E.A., Abatzoglou, J., Wilson, B.E., Breshears, D.D., Henebry, G.M., Hanes, J.M. and Liang, L. (2009). Tracking the rhythm of the seasons in the face of global change: phenological research in the 21st century. *Frontiers in Ecology and the Environment*, 7(5), pp.253-260. https://doi.org/10.1890/070217

Morisette, J. T., Duffy, K. A., Weltzin, J. F., Browning, D. M., Marsh, R. L., Friesz, A. M., … Richardson, A. D. (2021). PS3: The Pheno-Synthesis software suite for integration and analysis of multi-scale, multi-platform phenological data. *Ecological Informatics*, *65*, p. 101400. https://doi.org/10.1016/j.ecoinf.2021.101400

Morris, D. E., Boyd, D. S., Crowe, J. A., Johnson, C. S., & Smith, K. L. (2013). Exploring the potential for automatic extraction of vegetation phenological metrics from traffic webcams. *Remote Sensing*, 5(5), 2200–2218. https://doi.org/10.3390/rs5052200

Nagai, S., Akitsu, T., Saitoh, T. M., Busey, R. C., Fukuzawa, K., Honda, Y., … Nasahara, K. N. (2018). 8 million phenological and sky images from 29 ecosystems from the Arctic to the tropics: the Phenological Eyes Network. *Ecological Research,* 1–2. https://doi.org/10.1007/s11284-018-1633-x

National Phenological Network. (2008). Developing a Plant Profile, 20-22. https://www.usanpn.org/files/articles/developing_a_plant_profile.pdf

Nguyen, H. ; Huete, A. R. ;Ebert, E. E. ; Beggs, P. ; Emmerson, K. ;Silver, J. ;Davies, J.(2018) Improving the spatio-temporal characterization of grass flowering in Australian rainfed grasslands using digital time-lapse photography and landscape phenology from Sentinel-2 and MODIS. *AGU meeting*, abstract #B055-05

NOAA. https://w2.weather.gov/climate/index.php?wfo=bou

Nowak, D.J., Hoehn R.E., Stevens, J.C., Fisher, C.L. (2010). *Assessing Urban Forest Effects and Values: Chicago's urban forest.* USDA Forest Service, Delaware OH.

Okigbo, C. A., Seeam, A., Guness, S. P., Bellekens, X., Bekaroo, G., & Ramsurrun, V. (2020). Low cost air quality monitoring: Comparing the energy consumption of an arduino against a raspberry Pi based system. *ACM International Conference Proceeding Series*. 36, 1-2. https://doi.org/10.1145/3415088.3415124

Oregon Research Electronics. http://www.orelectronics.net/products/

ORE Manual, page 10. (2020). http://www.orelectronics.net/wp-content/uploads/2020/11/AL101-Manual-V6.pdf

967 Ottosen, T. B., Ketzel, M., Skov, H., Hertel, O., Brandt, J., & Kakosimos, K. E. (2019). Micro-
968 scale modelling of the urban wind speed for air pollution applications. *Scientific Reports*,
969 *9*(1), 1–11. https://doi.org/10.1038/s41598-019-50033-2
970 Park, D. S., Newman, E. A., & Breckheimer, I. K. (2021). Scale gaps in landscape phenology:
971 challenges and opportunities. *Trends in Ecology and Evolution*, 36(8), 709–721.
972 https://doi.org/10.1016/j.tree.2021.04.008
973 Poland, T. M., & Mccullough, D. G. (2006). EAB Invasion of the Urban Forest and the threat to
974 North America's ash resource. *Journal of Forestry*; April-May, 2006:118–124.
975 Primack, R.B., Higuchi, H., Miller-Rushing, A.J. (2009). The impact of climate change on cherry
976 trees and other species in Japan. *Biol. Conserv*. 142, 1943e1949.
977 10.1016/j.biocon.2009.03.016
978 Pusey, P. L., & Curry, E. A. (2007). Temperature and Pomaceous Flower Age Related to
979 Colonization by *Erwinia amylovora* and Antagonists. *Phytopathology,* 94(8), 901–911.
980 https://doi.org/10.1094/phyto.2004.94.8.901
981 R Core Team. (2021). R: A language and environment for statistical computing. R Foundation
982 for Statistical Computing, Vienna, Austria. URL http://www.R-project.org/.
983 Raleigh, M.S., Gutmann, E.D., Van Stan II, J.T., Burns, S.P., Blanken, P.D., and E.E. Small.
984 Challenges and capabilities in estimating snow mass intercepted in conifer canopies with
985 tree sway monitoring [PrePrint]. https://essoar.org (2021)
986 https://doi.org/10.1002/essoar.10507747.2

987 Richardson, A. D., Hufkens, K., Milliman, T., Aubrecht, D. M., Furze, M. E., Seyednasrollah, B.,
988 … Hanson, P. J. (2018). Ecosystem warming extends vegetation activity but heightens
989 vulnerability to cold temperatures. *Nature*, *560*(7718), 368–371.
990 https://doi.org/10.1038/s41586-018-0399-1

991 Richardson, A. D., Weltzin, J.F, Morisette. J.T. (2017), Integrating multiscale seasonal data for
992 resource management*, Eos,* 98, https://doi.org/10.1029/2017EO065709.
993 Sano M, Nakagawa Y, Sugimoto T, Shirakawa T, Yamagishi K, Sugihara T, Ohaba M,
994 Shibusawa S. 2015. Estimation of water stress of plant by vibration measurement of leaf
995 using acoustic radiation force. *Acoustical Science and Technology,* 36, 248–253.
996 https://doi.org/10.1250/ast.36.248
997 Schindler, D., Schönborn, J., Fugmann, H., & Mayer, H. (2013). Responses of an individual
998 deciduous broadleaved tree to wind excitation. *Agricultural and Forest Meteorology,* 177,
999 69–82. https://doi.org/10.1016/J.AGRFORMET.2013.04.001
1000 Schwartz M, Hanes J. 2010. Intercomparing multiple measures of the onset of spring in
1001 eastern North America. *International Journal of Climatology*, 30: 1614-1626.
1002 https://doi.org/10.1002/joc.2008
1003 Selker, J.S., Lane, J.W., Rupp, D.E., Hut, R., Abou Najm, M.R., Stewart, R.D., et al. (2011). The
1004 answer is blowing in the wind: using wind induced resonance of trees to measure time
1005 varying canopy mass, including interception. *AGU Fall Meet.* Abstr. 11.
1006 Seyednasrollah, B., Milliman, T., & Richardson, A. D. (2019). Data extraction from digital repeat
1007 photography using xROI: An interactive framework to facilitate the process. *ISPRS*
1008 *Journal of Photogrammetry and Remote Sensing*, 152, 132–144.
1009 https://doi.org/10.1016/J.ISPRSJPRS.2019.04.009
1010 Skywatch weather archive. (2018). University of Colorado Boulder ATOC weather network.
1011 https://sundowner.colorado.edu/weather/atoc8/archive_index.html
1012 Spatz, H.C. and Theckes, B. (2013). Oscillation damping in trees. *Plant Sci.* 2013, 207, 66–71
1013 Sunoj, S., Igathinathane, C., & Hendrickson, J. (2016). Monitoring plant phenology using
1014 phenocam: A review. 2016 *American Society of Agricultural and Biological Engineers*
1015 *Annual International Meeting*, ASABE 2016, (September 2020).
1016 https://doi.org/10.13031/aim.20162461829

1017 Stanley, C. H., Helletsgruber, C., & Hof, A. (2019). Mutual Influences of Urban Microclimate and
1018 Urban Trees: An Investigation of Phenology and Cooling Capacity. *Forests* 2019, Vol.
1019 10, Page 533, 10(7), 533. https://doi.org/10.3390/F10070533
1020 Sturm, J. T., Sturm, J. T., De Jong, R., & Schaepman, M. E. (2018). Extraction of general
1021 flowering metrics in Malaysian Borneo using optical indices on phenocam images. *ESA*
1022 *Conference Abstract*, New Orleans, LA
1023 Traidl-Hoffmann C, Kasche A, Menzel A, Jakob T, Thiel M, Ring J, Behrendt H. 2003. Impact of
1024 pollen on human health: more than allergen carriers? *International Archives of Allergy*
1025 *and Immunology*, 131: 1–13. 10.1159/000070428
1026 Tryjanowski, P., Sparks, T.H., Kúzniak, S., Czechowski, P., Jerzak, L., 2013. Bird migration
1027 advances more strongly in urban environments. *PLoS One,* 8 (5), e63482.
1028 https://doi.org/10.1371/journal.pone.0063482
1029 Tzoulas, K., Korpela, K., Venn, S., Yli-Pelkonen, V., Kamierczak, A., Niemela, J., & James, P.
1030 (2007). Promoting ecosystem and human health in urban areas using Green
1031 Infrastructure: A literature review. *Landscape and Urban Planning*, 81, 167–178.
1032 https://doi.org/10.1016/j.landurbplan.2007.02.001
1033 van Emmerik, T., Steele-Dunne, S., Hut, R., Gentine, P., Guerin, M., Oliveira, R., et al. (2017).
1034 Measuring tree properties and responses using low-cost accelerometers. *Sensors,* 17,
1035 1098. 10.3390/s17051098
1036 Vaz, A. S., Gonçalves, J. F., Pereira, P., Santarém, F., Vicente, J. R., & Honrado, J. P. (2019).
1037 Earth observation and social media: Evaluating the spatiotemporal contribution of non-
1038 native trees to cultural ecosystem services. *Remote Sensing of Environment*, 230(June
1039 2018), 111193. https://doi.org/10.1016/j.rse.2019.05.012
1040 Verdugo-Vásquez, N., Acevedo-Opazo, • C, Valdés-Gómez, • H, Araya-Alman, • M, Ingram, • B,
1041 García De Cortázar-Atauri, • I, … Cl, C. (2016). Spatial variability of phenology in two

irrigated grapevine cultivar growing under semi-arid conditions. *Precision Agric,* 17, 218–245. https://doi.org/10.1007/s11119-015-9418-5

Walther GR, Post E, Convey P, Menzel A, Parmesan C, Beebee TJC, Fromentin JM, Hoegh-Guldberg O, Bairlein F. 2002. Ecological responses to recent climate change. *Nature,* 416: 389–395. 10.1038/416389a

Wang, L., Ning, Z., Wang, H., & Ge, Q. (2017). Impact of Climate Variability on Flowering Phenology and Its Implications for the Schedule of Blossom Festivals. *Sustainability,* 2017, Vol. 9, Page 1127, 9(7), 1127. https://doi.org/10.3390/SU9071127

Wolhfahrt, G., Tomelleri, E., & Hammerle, A. (2019). The urban imprint on plant phenology. *Nature Ecology & Evolution,* 2019 3:12, 3(12), 1668–1674. https://doi.org/10.1038/s41559-019-1017-

Xiao, Q. and McPherson, E.G. (2002). Rainfall interception by Santa Monica's municipal urban forest. *Urban Ecosyst.,* 6, 291–302. https://doi.org/10.1023/B:UECO.0000004828.05143.67

Yang, J., Luo, X., Jin, C., Xiao, X., & Xia, J. (2020). Spatiotemporal patterns of vegetation phenology along the urban–rural gradient in Coastal Dalian, China. *Urban Forestry and Urban Greening*, 54. https://doi.org/10.1016/j.ufug.2020.126784

Yingying, X. I. E., Civco, D. L., & Silander, J. A. (2018). Species-specific spring and autumn leaf phenology captured by time-lapse digital cameras. *Ecosphere*, 9(1):e02089. https://doi.org/10.1002/ecs2.2089

Zheng, J., Zhong, S., Quansheng, G. E., Zhixin, H., Zhang, X., & Xiang, M. A. (2013). Changes of spring phenodates for the past 150 years over the Yangtze River Delta. *J. Geogr. Sci*, 2013(1), 31–44. https://doi.org/10.1007/s11442-013-0991-0

Ziter, C. D., Pedersen, E. J., Kucharik, C. J., & Turner, M. G. (2019). Scale-dependent interactions between tree canopy cover and impervious surfaces reduce daytime urban

heat during summer. *Proceedings of the National Academy of Sciences*, 116(15), 7575–7580. https://doi.org/10.1073/pnas.1817561116